Available online at www.sciencedirect.com
SCIENCE DIRECT®
Computerized Medical Imaging and Graphics 27 (2003) 321–337
Computerized Medical Imaging and Graphics
www.elsevier.com/locate/compmedimag

3D/2D registration and segmentation of scoliotic vertebrae using statistical models

Said Benameur[a,b,c,*], Max Mignotte[a,b], Stefan Parent[d], Hubert Labelle[d], Wafa Skalli[e], Jacques de Guise[a,c,d]

[a]*Laboratoire de recherche en imagerie et orthopédie, Centre de recherche, Centre hospitalier Universitaire de Montréal, Pavilion J.A. de Sève 1560, rue Sherbrooke est, Montréal, Que., Y-1615, Canada H2L 4M1*
[b]*Laboratoire de vision et modélisation géométrique, Département d'informatique et recherche opérationnelle, Université de Montréal, Canada*
[c]*École de technologie supérieure, Montréal, Canada*
[d]*Laboratoire d'imagerie en scoliose 3D, Centre de recherche, Hôpital Sainte-Justine, Montréal, Canada*
[e]*Laboratoire de biomécanique, École nationale supérieure d'arts et métiers, Paris, France*

Received 13 May 2002; accepted 13 January 2003

Abstract

We propose a new 3D/2D registration method for vertebrae of the scoliotic spine, using two conventional radiographic views (postero-anterior and lateral), and a priori global knowledge of the geometric structure of each vertebra. This geometric knowledge is efficiently captured by a statistical deformable template integrating a set of admissible deformations, expressed by the first modes of variation in Karhunen–Loeve expansion, of the pathological deformations observed on a representative scoliotic vertebra population. The proposed registration method consists of fitting the projections of this deformable template with the preliminary segmented contours of the corresponding vertebra on the two radiographic views. The 3D/2D registration problem is stated as the minimization of a cost function for each vertebra and solved with a gradient descent technique. Registration of the spine is then done vertebra by vertebra. The proposed method efficiently provides accurate 3D reconstruction of each scoliotic vertebra and, consequently, it also provides accurate knowledge of the 3D structure of the whole scoliotic spine. This registration method has been successfully tested on several biplanar radiographic images and validated on 57 scoliotic vertebrae. The validation results reported in this paper demonstrate that the proposed statistical scheme performs better than other conventional 3D reconstruction methods.

Keywords: 3D/2D registration; 3D reconstruction model; Statistical deformable model; Shape model; Biplanar radiographies; Scoliosis; Medical imaging; Energy function optimization

1. Introduction

Registration, an important problem in computer vision, is still incompletely solved. It primarily consists of establishing a geometric relation between the objects represented by two images. Many methods of image registration have been proposed in the literature (see, for example, a good survey of image registration methods proposed by Brown in Ref. [1], and the excellent review of existing registration techniques proposed by Van den elsen et al. in Ref. [2], Lavallée in Ref. [3], or Maintz and Viergever in Ref. [4], specific to the medical image registration problem). A comparison between several registration approaches has been also undertaken by West in Ref. [5].

Registration is a problem common to many tasks in medical imagery. Among these tasks, we can cite the 3D reconstruction of anatomical structures, the fusion of information coming from several methods, the construction of anatomical and functional atlases in medical imaging (allowing the detection of local and/or anatomical or functional abnormalities), the voluminal and dynamic visualization of images, etc.

In our application, we use a 3D/2D statistical registration model from biplanar radiographic images for the 3D

* Corresponding author. Address: Laboratoire de recherche en imagerie et orthopédie, Centre de recherche, Centre hospitalier Universitaire de Montréal, Pavilion J.A. de Sève 1560, rue Sherbrooke est, Montréal, Que., Y-1615, Canada H2L 4M1. Tel.: +1-514-890-8000; fax: +1-514-412-7785.
E-mail address: benameus@iro.umontreal.ca (S. Benameur).

0895-6111/03/$ - see front matter © 2003 Elsevier Science Ltd. All rights reserved.
doi:10.1016/S0895-6111(03)00019-3

reconstruction of scoliotic vertebrae of a spine. Scoliosis is a 3D deformation of the natural curve of the spinal column, including rotations and vertebral deformations. To analyze the 3D characteristics of these deformations, which can be useful for the design, evaluation and improvement of orthopedic or surgical correction, several 3D reconstruction methods have been developed. The 3D reconstruction methods of tomodensitometric imagery modalities (e.g. X-rays, magnetic resonance) provide accurate 3D information of the human anatomy. However, the high level of radiation received by the patient, the large quantity of information to be acquired and processed, and the cost of these methods make them less functional [6]. 3D reconstruction methods using a limited number of projections and some simple a priori knowledge of the geometry of the object to be reconstructed are interesting but are widely supervised; for example they may require manual identification (by an operator) of a set of 19 different points of interest (landmarks) on two different radiographic images (postero-anterior (I_{PA}) and lateral (I_{LAT})) of 17 lumbar and thoracic vertebrae [6–8]. Besides, these aforementioned methods may not be very accurate, especially because they do not exploit all the information contained in the two radiographic images (e.g. the contours of each vertebra or a priori global geometrical knowledge of the object to be reconstructed), and because they are highly operator-dependent. To this end, Bayesian inference or statistical modeling is a convenient way of taking a priori information into consideration. The statistical approach is quite popular and has been successfully applied in medical imagery [9–11], in image analysis for extracting 2D objects in an image [12] or in an image sequence [13], for the 3D representation of vertebra [14], non-rigid 3D/2D registration of the knee [15,16], segmentation of 2D anatomical structures [17–20], localization and classification [21], etc.

In this way, we propose a new 3D/2D registration modeling approach for scoliotic vertebrae from biplanar radiographic images which can be viewed as a new statistical 3D reconstruction method. Our approach relies on the description of each vertebra by a deformable 3D template which incorporates (statistical) knowledge about its geometrical structure and its pathological variability. The deformations of this template are expressed by the first modes of variation in Karhunen–Loeve (KL) expansion of the pathological deformations observed on a representative scoliotic vertebra population. This prototype template, along with the set of admissible deformations, constitutes our global a priori model that will be used to rightly constraint the ill-posed nature of our 3D/2D registration problem [22]. In our application, the proposed method consists of fitting this template with the segmented contours of the corresponding vertebra on two calibrated radiographic views. This matching problem leads to an optimization problem of a cost function, efficiently solved in our application by a gradient descent algorithm initialized by a rough and rigid 3D/2D registration method estimated in the least square sense.

This paper is organized as follows. Section 2 presents the statistical deformable model. Section 3 describes the proposed 3D/2D registration method. Section 4 discusses the validation protocol of our method. The experimental results of our 3D/2D registration or 3D reconstruction method are presented in Section 5. Finally, we conclude the paper in Section 6 with a discussion and perspectives.

2. Statistical deformable model

The shape s of each vertebra is defined by a set of n control points or 'landmarks', which approximate the geometric shape of each vertebra in IR^3 [12]. Each vertebra, in the training set, is thus represented by the following $3n$ dimensional vector

$$s = (p_1 p_2 \ldots p_i \ldots p_n)^{\mathrm{T}},$$

where $P_i = (x_i y_i z_i)^{\mathrm{T}}$ are the Cartesian coordinates of each surface point. In the following, we will assume that s is the realization of a random vector that follows a normal law of mean vector $\bar{s}$ and covariance matrix C, as suggested in [12]. After alignment of the N training shapes [12], mean shape and the covariance matrix are defined as,

$$\bar{s} = \frac{1}{N}\sum_{i=1}^{N} s_i, \qquad C = \frac{1}{N}\sum_{i=1}^{N} (s_i - \bar{s})(s_i - \bar{s})^{\mathrm{T}}.$$

The variabilities within the training set are characterized by the displacement vector $\tilde{s} = s - \bar{s}$ of the different surface points with respect to the mean model. Statistical analysis of this random vector makes it possible to deduce the deformation modes relative to the mean shape. The eigenvectors of the covariance matrix C of this random vector describe the variation modes in the deformation parameter space or information on the variability of scoliotic deformations in the vertebra database. The associated eigenvalues λ_i are the amplitudes of these variation modes. An accurate description of the main variation modes may be obtained by retaining only the t eigenvectors associated with the t largest eigenvalues[1] [12]. The model allows the generation of new instance of the shape by adding linear combinations of the t most significant variation vectors to the mean shape,

$$s = \bar{s} + \phi b, \tag{1}$$

where ϕ represents an orthogonal base of variation modes of scoliotic vertebrae contained in the training base, and b is the global deformation parameter vector setting the

[1] As C is symmetric ($C^{\mathrm{T}} = C$), its eigenvalues are real and the associated eigenvectors are orthogonal. As C is positive definite, its eigenvalues are positive or null.

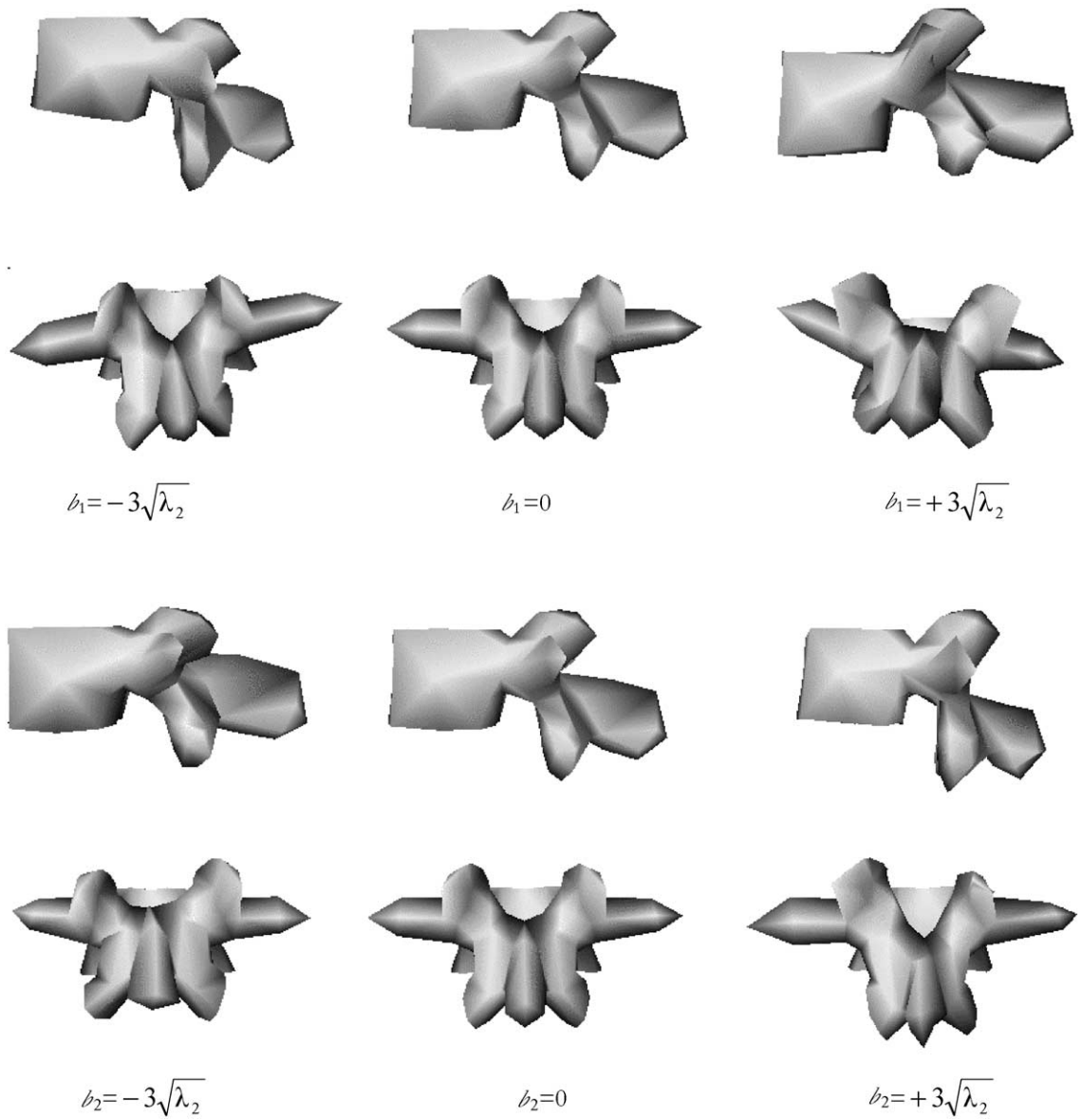

Fig. 1. Visualization of mean shape (middle row) from the sagittal (top row) and coronal views (bottom row), and two deformed shapes obtained by applying ±3 standard deviations of the first and second deformation modes to the mean shape for the L3 vertebra.

amplitudes of each deformation mode b_i. By ensuring,

$$-3\sqrt{\lambda_i} \leq b_i \leq +3\sqrt{\lambda_i}, \tag{2}$$

where λ_i is the eigenvalue associated with the deformation mode b_i, only the important deformations are extracted, discarding training data noise [12]. This low parametric representation of a vertebra constitutes our global a priori model that will be used in our 3D reconstruction method (Figs. 1–2).

In theory, the ratio of an eigenvalue to the total sum of the other eigenvalues expresses the percentage of error introduced if the eigenvector associated with the corresponding eigenvalue is not selected [12]. One must thus specify a threshold $f_v (f_v \in [0, 1])$ for the eigenvalues above which the error is considered to be sufficiently small to generate a good approximation of the initial vector. Hence, if V_T is the sum of the eigenvalues, then the number t of eigenvalues to be selected is such that,

$$\sum_{i=1}^{t} \lambda_i \geq f_v V_T.$$

By doing so, we ensure that the selected deformation modes allow us to represent $100f_v\%$ of the existing scoliotic deformations in the training base.[2]

[2] Each vector can also be characterized by the Mahalanobis distance $(s-\bar{s})^{\mathrm{T}} C^{-1} (s-\bar{s})$ directly related to a normal distribution. From relation (2), we deduce that [12],

$$\sum_{i=1}^{t} \frac{b_i^2}{\lambda_i} \leq 9t. \tag{3}$$

A random vector s which does not check this condition could be considered to be not representative with respect to statistical training. In practice, the criterion expressed by Eq. (3) could be used to validate certain configurations of shapes [17].

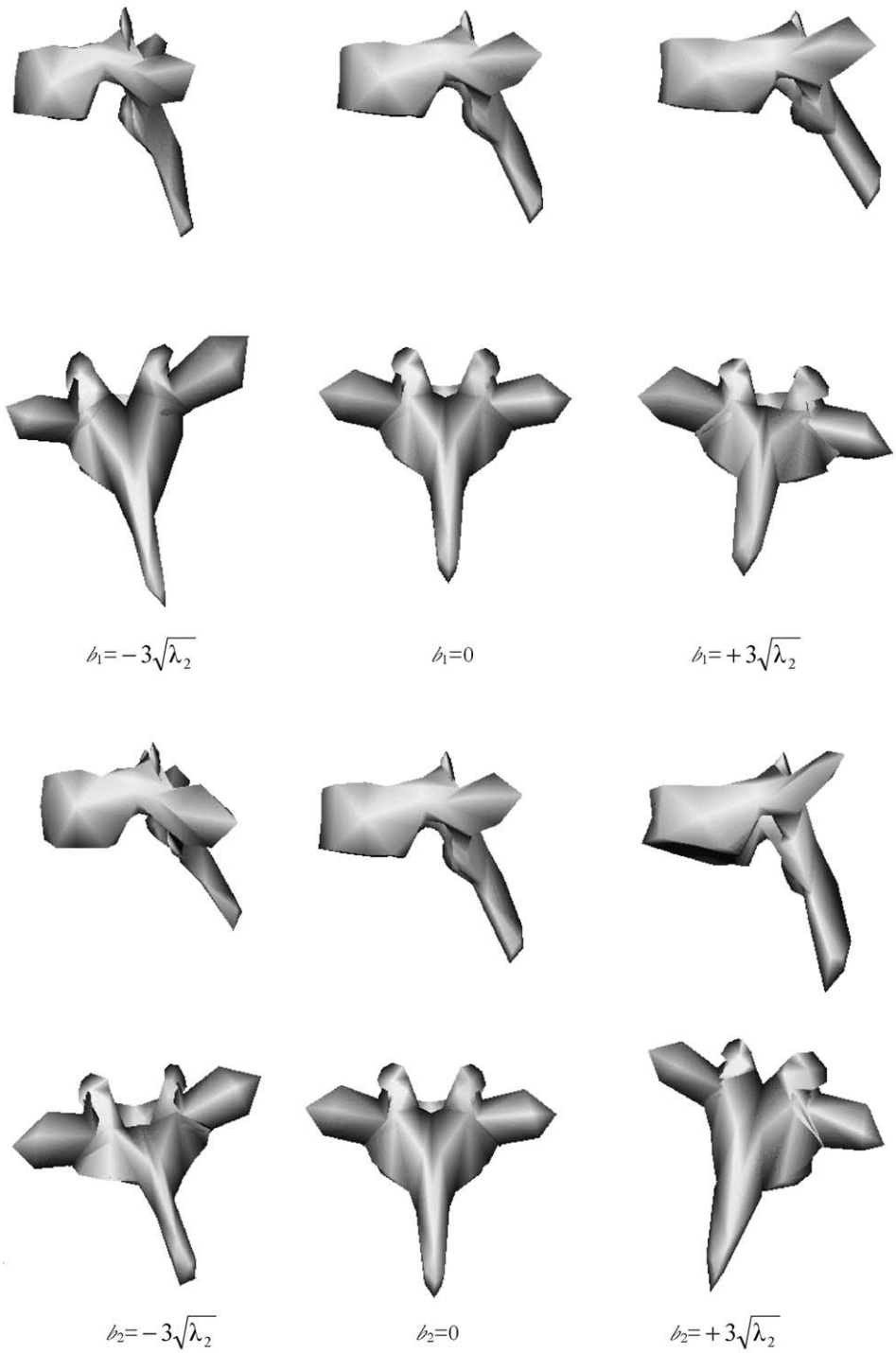

Fig. 2. Visualization of mean shape (middle row) from the sagittal (top row) and coronal views (bottom row), and two deformed shapes obtained by applying ± 3 standard deviations of the first and second deformation modes to the mean shape for the T6 vertebra.

3. 3D/2D registration method

Besides the above-mentioned global deformation parameters, we also consider 3D global transformations from the similarity group which finally lead to the following model for global deformations,

$$s = M(k, \alpha)[\bar{s} + \phi b] + T,$$

with $k (k \geq 0)$ and α being, respectively, the scale and the rotation vector, and T is a global translation vector. The rotation matrix R can be represented by a product of three separate rotation matrixes $R_{\alpha 1}, R_{\alpha 2}$, and $R_{\alpha 3}$ which correspond to rotations around the x, y, and z axes, respectively ($\alpha_1, \alpha_2, \alpha_3 \in [0, 2\pi]$). The rotation matrix R and the global translation vector T are regrouped in

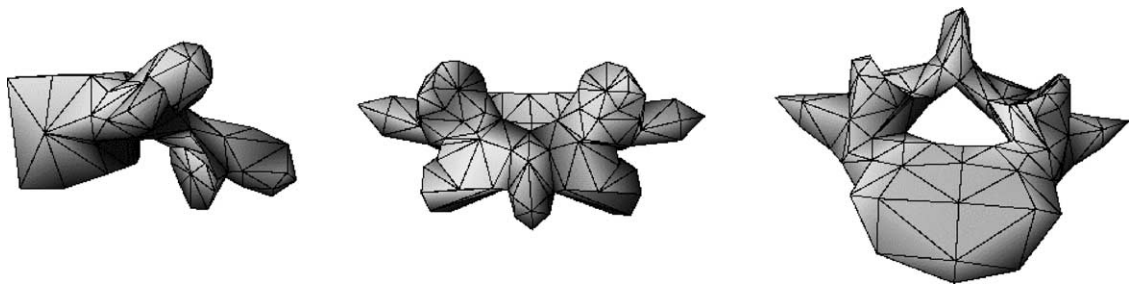

Fig. 3. Visualization of the shape model: sagittal, coronal and axial views.

the $3n \times 3n$ dimensional transformation matrix $M(k, \alpha)$ as follows,

$$M(k,\alpha) = \begin{pmatrix} M_1(k,\alpha) & 0 & \dots & 0 \\ 0 & M_2(k,\alpha) & \dots & 0 \\ \vdots & \vdots & \ddots & \vdots \\ 0 & 0 & \dots & M_n(k,\alpha) \end{pmatrix},$$

where $M_i(k, \alpha) = kR_{\alpha_3}R_{\alpha_2}R_{\alpha_1}$,

$$T = \begin{pmatrix} T_x \\ T_y \\ T_z \end{pmatrix},$$

and,

$$R_{\alpha 1} = \begin{pmatrix} 1 & 0 & 0 \\ 0 & \cos(\alpha_1) & -\sin(\alpha_1) \\ 0 & \sin(\alpha_1) & \cos(\alpha_1) \end{pmatrix},$$

$$R_{\alpha 2} = \begin{pmatrix} \cos(\alpha_2) & 0 & \sin(\alpha_2) \\ 0 & 1 & 0 \\ -\sin(\alpha_2) & 0 & \cos(\alpha_2) \end{pmatrix},$$

$$R_{\alpha 3} = \begin{pmatrix} \cos(\alpha_3) & -\sin(\alpha_3) & 0 \\ \sin(\alpha_3) & \cos(\alpha_3) & 0 \\ 0 & 0 & 1 \end{pmatrix}.$$

3.1. Crude and rigid initial registration

To ensure a first crude and rigid reconstruction of each vertebra, we use the technique proposed in [23]. This technique identifies, in a preliminary step, a sequence of eight points along the centerline of the spine from the C1 cervical vertebra to the L5 lumbar vertebra on the two radiographic views of the spine. These points are then exploited to determine the position of six anatomical points (namely, the center of the superior and inferior end-plates, the upper and lower extremities of both pedicles) for each vertebra of the spine (Fig. 4). The corresponding points on the shape of the mean vertebra being known, we can obtain, in the least square sense [24], an initial estimate of the parameter vector (α, T). This leads us to crude and rigid registration for each vertebra that will then be refined by our 3D reconstruction model.

3.2. 3D/2D model registration

Our reconstruction model from two radiographic views is stated as the minimization of the following cost function,

$$E(s,\theta) = E_{\mathrm{l}}(s, I_{\mathrm{PA}}, I_{\mathrm{LAT}}) + \beta E_{\mathrm{p}}(s), \tag{4}$$

where $E_{\mathrm{l}}(s, I_{\mathrm{PA}}, I_{\mathrm{LAT}})$ is the likelihood energy term, and $E_{\mathrm{p}}(s)$ is the prior energy term (or the regularization term), used to constrain the ill-posed nature of this optimization problem. β is a factor that provides relative weighting between the two penalty terms and allows us to control the rigidity of the statistical template [25]. $\theta = (M(k, \alpha), T, b)$ is the deformation parameter vector of the model to be estimated. It should be noted that this optimization problem can also be formulated as the search for the maximum a posteriori (MAP) of θ, the deformation parameters of the deformed template s,

$$s^* = \arg\max_s P(I_{\mathrm{PA}}, I_{\mathrm{LAT}}|s)P(s), \tag{5}$$

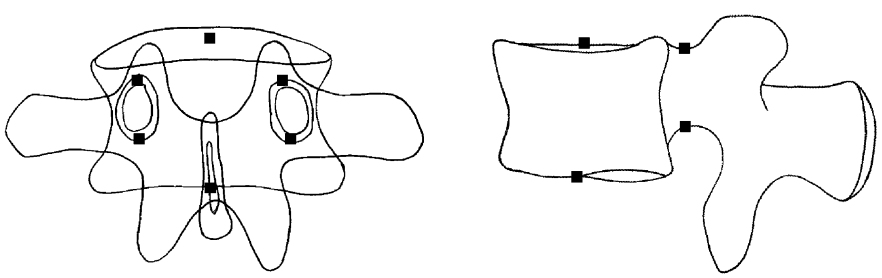

Fig. 4. Anatomical stereo-corresponding landmarks.

where

$$P(I_{PA}, I_{LAT}|s) = \frac{1}{\mathscr{Z}_l}\exp(-E_l(s, I_{PA}, I_{LAT}))$$

is the likelihood of the observations (i.e. the segmented contours on the two radiographic views) given by a deformed template, and

$$P(s) = \frac{1}{\mathscr{Z}_p}\exp(-E_p(s))$$

is the prior probability of the deformed template (or the prior probability of a scoliotic deformation for a given vertebra). $\mathscr{Z}_l$ and $\mathscr{Z}_p$ are two constants of normalization.

3.3. Likelihood energy term

In our application, our likelihood model is expressed by a measure of similarity between the external contour of the lateral and the postero-anterior perspective projections of the deformed template and an *edge potential field* estimated on the two radiographic views. First, this edge potential field requires the preliminary detection of edges in the two radiographic images. To do so, we use a simple Canny edge detector [26]. Second, this field is determined by the positions of the detected edges in the radiographic images. For a pixel (x, y) in the postero-anterior or lateral image, we define its edge potential by,

$$\psi(x, y) = \exp\left(-\frac{\sqrt{\xi_x^2 + \xi_y^2}}{\tau}\right),$$

where (ξ_x, ξ_y) is the displacement to the nearest edge point in the image, and τ is a smoothing factor which controls the degree of smoothness of this potential field.[3] This edge potential induces an energy function that relates a deformed template s to the edges in the two radiographic images I_{PA} and I_{LAT} (Fig. 11)

$$E_l(s, I_{PA}, I_{LAT}) = -\frac{1}{n_{PA}}\sum_{\Gamma_{PA}}\psi_{PA}(x, y) - \frac{1}{n_{LAT}}\sum_{\Gamma_{LAT}}(x, y), \quad (6)$$

where the summation of the first and second term of $E_l(s, I_{PA}, I_{LAT})$ is overall the n_{PA} and n_{LAT} of the external contour of the, respectively, lateral and postero-anterior perspective projections of the deformed template on the two pre-computed edge potential fields of each radiographic image. This energy function attains its minimum value when there is an exact correspondence between the projected contours (of the deformed template) and the preliminary segmented contours of the two radiographic views.

3.4. Prior energy term

Due to KL transformation, the random variables b_i are independent and follow a normal law of a null mean and variance λ_i [12]. Thus, the law of probability of s, the deformed template, can be written as [13],

$$P(s) = \prod_{i=1}^{t}\frac{1}{\sqrt{2\lambda_i\pi}}\exp\left(-\frac{b_i^2}{2\lambda_i}\right).$$

This probability expresses the fact that the shape to be reconstructed is likely close to the mean shape. By considering that

$$P(s) = \frac{1}{\mathscr{Z}_p}\exp(-E_p(s)),$$

the prior energy term can be written as,

$$E_p(s) = \frac{1}{2}\sum_{i=1}^{t}\frac{b_i^2}{\lambda_i}. \quad (7)$$

This energy term penalizes the deviation of the deformed template from the mean shape. This term does not penalize affine transformations. Eq. (7) closely resembles the Mahalanobis distance. It defines an ellipsoid centered in IR^t whose principal axes are identified by $\sqrt{\lambda_i}$ when $E_p(s)$ is a constant.

3.5. Silhouette extraction of the 3D model

The 3D model of vertebrae is represented in the form of a triangulated mesh (Fig. 5) Silhouette detection is based on estimation of the normal at each vertex of the mesh. The normal in each vertex is computed by the average of the normal of all facets to which the vertex belongs (Fig. 6). For two neighbours V_1 and V_2 of facet F_i whose product of the weights is negative, we interpolate linearly along the edge (V_1V_2) (Table 2). The line joining two interpolated vertices of F_i is called the external edge (Fig. 7). On a surface Γ, the external edges of the vertebra shape are lines where the direction of projection is tangent on the surface [27,28]. The external edges are saved in a list. As in the case of a not-convex object, the external edges can be hidden by other parts of the surface. We keep all the external edges, including those that are occulted (i.e. those that are hidden by another part of the vertebra). Let us recall that we use semi-transparent radiographic images (i.e. superposition of the various structures on a the same plan). In our application, occulted edges are also exploited in our 3D/2D registration method. Let us put all the external edges having a joint vertex in a list. Each one of these lists constitutes an external contour of the vertebra. The set of these external contours constitutes the silhouette of

[3] We can easily complete this edge potential field $\psi(x, y)$ by adding to it a directional component to obtain a directional edge potential field,

$$\psi'(x, y) = \psi(x, y)|\cos(\gamma(x, y))|,$$

where $\gamma(x, y)$ is the angle between the tangent of the nearest edge and the tangent direction of the contour at (x, y). This potential field is similar to the one proposed in Ref. [25] for a template-based localization approach.

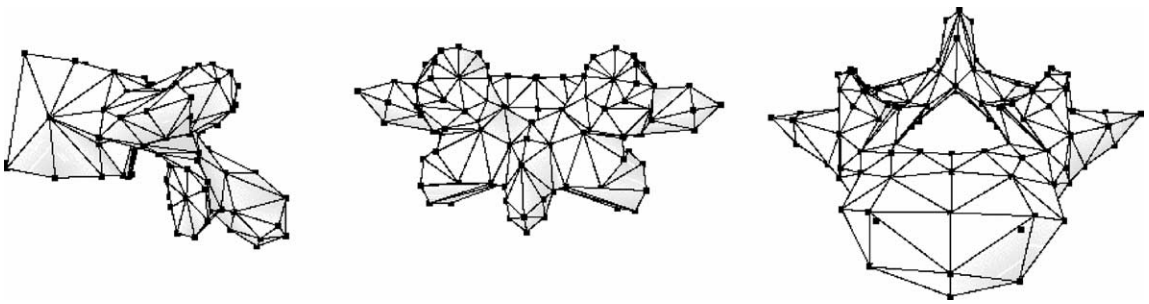

Fig. 5. Model of vertebra: triangulated mesh (187 points and 378 triangles).

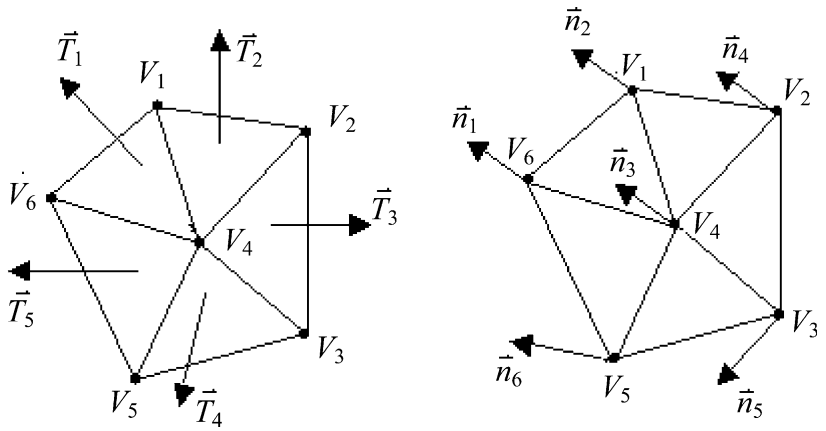

Fig. 6. Normal at the triangles, normal at the points.

the vertebra (Fig. 8). We summarize the whole procedure in Table 2.

3.6. Optimization of the energy function

The energy function to be minimized, namely,

$$E(s,\theta) = -\frac{1}{n_{\mathrm{PA}}}\sum_{\Gamma_{\mathrm{PA}}}\psi_{\mathrm{PA}}(x,y) - \frac{1}{n_{\mathrm{LAT}}}\sum_{\Gamma_{\mathrm{LAT}}}\psi_{\mathrm{LAT}}(x,y) + \beta\frac{1}{2}\sum_{i=1}^{t}\frac{b_i^2}{\lambda_i}, \quad (8)$$

is a complex function with several local minima over the deformation parameter space. A global search is impossible due to the size of the configuration space. In our application, experiments have shown that the initial crude and rigid reconstruction technique described in Section 3.1 (i.e. the estimation of rigid deformation parameters) can be efficiently exploited to initialize a gradient descent technique.

Various types of gradient descent have been used for rigid registration [29–32]. For our application, we combine the gradient descent technique with the strategy described in [25], which consists of sampling, out of θ, function $E(s,\theta)$ and using various samples obtained to initialize a local gradient descent technique. In our case,

Table 1
Algorithm used for fitting two 3D meshes

Fitting algorithm of two 3D mesh points

$V_{\mathrm{scan\_vert}}$: set of vertex of scanned vertebra
$V_{\mathrm{reco\_vert}}$: set of vertex of reconstructed vertebra
$V^{\mathrm{corresp}}_{\mathrm{scan\_vert}}$: set of corresponding vertex of scanned vertebra
$V^{\mathrm{corresp}}_{\mathrm{reco\_vert}}$: set of corresponding vertex of reconstructed vertebra
$V^{\mathrm{nearest}}_{\mathrm{scan\_vert}}$: empty set
ϵ : threshold
R : rotation
T : translation
Quaternions: quaternions algorithm

Initialization
$[R,T]$ = quaternions $(V^{\mathrm{corresp}}_{\mathrm{reco\_vert}}, V^{\mathrm{corresp}}_{\mathrm{scan\_vert}})$
To apply the rigid transformation (rotation R and translation T) to $V_{\mathrm{vert\_reco}}$

Optimization
$j = 0$; $\sum_0 = 0$;
While $|\sum_{j+1} - \sum_j| > \epsilon$
For each vertex V_i of $V_{\mathrm{reco\_vert}}$
Compute the nearest point N_i of V_i in $V_{\mathrm{scan\_vert}}$ and add N_i to $V^{\mathrm{nearest}}_{\mathrm{scan\_vert}}$
$[R,T]$ = quaternions $(V^{\mathrm{corresp}}_{\mathrm{reco\_vert}}, V^{\mathrm{nearest}}_{\mathrm{scan\_vert}})$
Apply the rigid transformation (rotation R and translation T) to $V_{\mathrm{vert\_reco}}$
Compute $\sum_j^2 = \sum_{i=1}^{n} \left\| V^{\mathrm{nearest}}_{\mathrm{scan\_vert}_i} - V_{\mathrm{reco\_vert}_i} \right\|^2$
End
Retain the rigid transformation (rotation R and translation T) corresponding at the last step

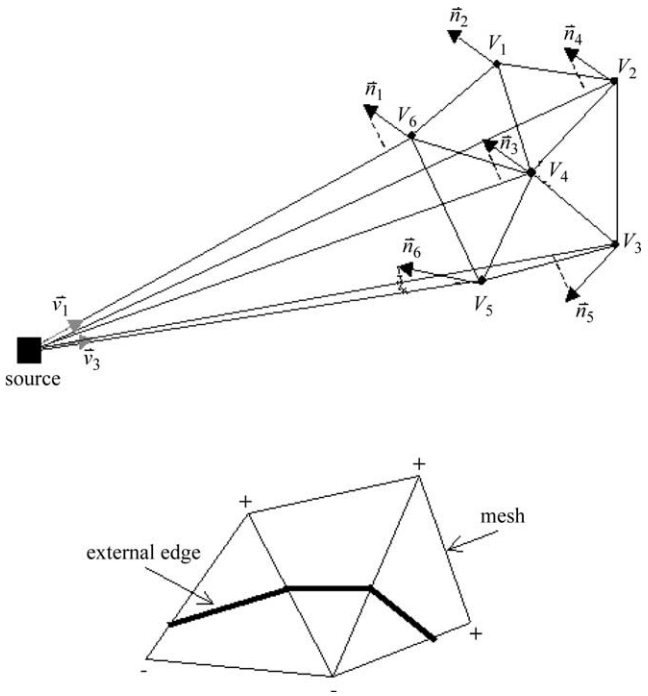

Fig. 7. Example of an external edge, the + and − signs on the vertices indicate the signs of its weights.

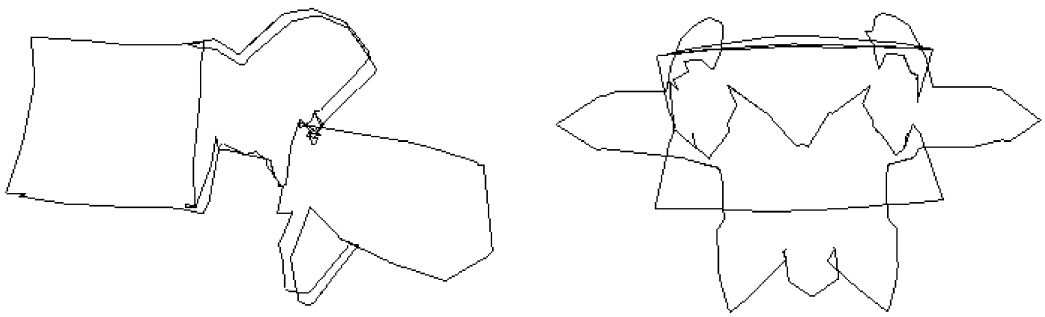

Fig. 8. Example of lateral and postero-anterior silhouettes of a vertebra given by the silhouette extraction algorithm.

we sample out function $E(s, \theta)$ around estimations given by the crude and rigid reconstruction technique presented in Section 3.1. The final adopted solution is the one associated with the lowest energy. However, the sampling of these template positions and transformation parameters must be chosen judiciously. It should be fine enough not to miss the significant local minima of the energy function, and large enough to avoid high computational requirements. In our application, we also use a simplified version of the traditional gradient descent technique, which does not require an analytical expression of the gradient of $E(s, \theta)$ (clearly unavailable in our case), and similar to the one proposed in [33]. We have summarized the whole procedure in Table 3. This gradient descent technique, combined with the above-mentioned sampling strategy, is deployed to simultaneously refine the estimation of rigid parameters and to estimate nonrigid parameters.

Table 2
Algorithm used for silhouette extraction

Silhouette extraction algorithm
$M = (V, F)$: mesh such that
$V : V = \{V_1, V_2, ..., V_i, ...V_n\} \subset \mathrm{IR}^3$ set of vertices
$F : F = \{F_1, F_2, ...F_i, ...F_m\}$ set of facets
L: Empty list
$\vec{n}_i$: normal in vertex V_i of facet F_i
$\vec{v}_i$: unit vector line joining the projection source and vertex V_i
For each facet F_i of F
Compute the normal at facet F_i
For each vertex V_i of V
Compute the normal at vertex V_i and its weight $\vec{n}_i \cdot \vec{v}_i$
For each facet F_i of F
For each pair of vertex $(V_i V_j)$ of F_i
If $(\vec{n}_i \cdot \vec{v}_i) \times (\vec{n}_j \cdot \vec{v}_j) < 0$ then
Interpolate linearly along the edge $(V_i V_j)$
Add the edge joining two interpolate points to L
Gather all the edges of L having a joint vertex in list L_i $(L = \{L_i / i \geq 0\})$

Table 3
Deterministic algorithm used for optimization of the energy function [33]

Gradient descent algorithm
E : energy function
θ : the deformation parameter vector
$\Delta\theta_i$: Step of each parameter
Sampling in θ of function $E(s, \theta)$ around the estimation given by the rigid reconstruction technique (cf. Section 3.1)
For each configuration or sample obtained
For each parameter $\theta_i (1 < i < t)$
Evaluate:
$E(\theta_1, ..., \theta_i - \Delta\theta_i, ..., \theta_t)$
$E(\theta_1, ..., \theta_i, ... \theta_t)$
$E(\theta_1, ..., \theta_i + \Delta\theta_i, ..., \theta_t)$
Retain the configuration θ associated with the lowest energy
We stop the algorithm for this sample when $E(s, \theta)$ is stable and the estimate obtained is memorized if the computed energy is lower than the last better estimate

4. Validation of 3D/2D registration

In our application, our 3D/2D registration technique is validated by comparing the reconstructed model obtained by our method and by reconstruction from CT-scan slices [34] by SliceOmatic© (TomoVision. http://www.tomovision.com/) software. 3D reconstruction models of the vertebrae contain up to 7,000 points per vertebra and will constitute the ground truth for our validation procedure. First, the validation procedure consists of fitting the model of 200 points of our 3D/2D registration method on the scanned vertebra. To this end, we manually extract some easily identifiable anatomical landmarks on the reconstructed model resulting from CT-scan whose position is known, and we estimate the rigid transformation allowing us to pass from the set of anatomical landmarks of our reconstructed model to the set of corresponding anatomical landmarks on the scanned model. Then, we apply this rigid transformation to all points of the reconstructed vertebra. Once this is done, we optimize the rigid transformation, which enables us to readjust the two models of vertebra. Optimization consists of finding neighbours on the scanned vertebra to each point of the reconstructed vertebra and then to estimating and re-applying the rigid deformation, allowing us to pass from the set of points of the reconstructed vertebra to the set of points close to the scanned vertebra.

The variation of error between the two sets of points is also computed.[4] This procedure is repeated until the difference in variation of error between two successive stages is lower than a given threshold.

The whole procedure is summarized in Table 1. We can exploit this 3D/2D registration method to estimate the mean and the maximum error distance between the 3D reconstructed model from our method and the 3D model resulting from CT-scan.

5. Experimental results

5.1. Vertebra database

The vertebra database consists of 1,020 thoracic and lumbar vertebrae (510 normal and 510 scoliotic). These data were obtained by digitization of the anatomical points on anatomical specimens. These anatomical specimens have been selected from the Hamann–Todd osteology collection of over 1,800 complete specimens in Cleveland, USA, and from the Robert J. Terry anatomical skeletal collection of over 1,700 specimens at the Smithsonian Institution in Washington, DC, USA[5] [39].

Fastrack© (POLHEMUS, A Rockwell Collins Company, http://www.polhemus.com/ftrakds.htm) is the name of the electromagnetic device used to digitize each vertebra by means of a pointer. The accuracy of this device is evaluated at ± 0.2 mm [40]. The 3D coordinates of the pointer were recorded in a specific reference system. The digitizing protocol consisted of measuring specific anatomical landmarks on each vertebra, thus creating a set of approximately 200 points depending on the level measured with regard to its particular geometry [41]. Different points were acquired in a specific order and recorded in this sequence. After the measurements were done, each vertebra was then reconstructed using computer graphics software. Each set of points was then re-localized in a local coordinate system.[6]

5.2. Radiographic images

In our application, we used two radiographic images (i.e. postero-anterior and lateral) acquired with a Fuji FCR 7501S radiographic imaging system. Radiography is the image in 2D projection of a 3D object whose X-rays are the source of illumination. The intensity transmitted through a specific zone of an object decreases according to the nature and thickness of the material through which radiation passes. Thus, air, soft tissue (muscles, cartilage, etc.) and bones present different attenuation coefficients for X-rays and can, in this way, become theoretically localized in radiological images. Thus, the radiographic

[4] Many methods have been proposed in the literature to estimate the rigid transformations R and T. In Ref. [35], LORUSSO compared the quaternion method [24], polar decomposition [36], the method of decomposition in singular values (SVD) [37], and the duaux quaternion method [38]. This study concludes that the difference in precision is not significant, the computational times are comparable, and that the only substantial difference is the sensitivity of the algorithms when the points used approach a degenerated configuration. In our case, we use the quaternion method.

[5] Age, sex, race, height, weight, cause of death and peculiar dissection findings of each scoliotic specimen are available.

[6] To our knowledge, the vertebrae base is the largest database available in the literature [39].

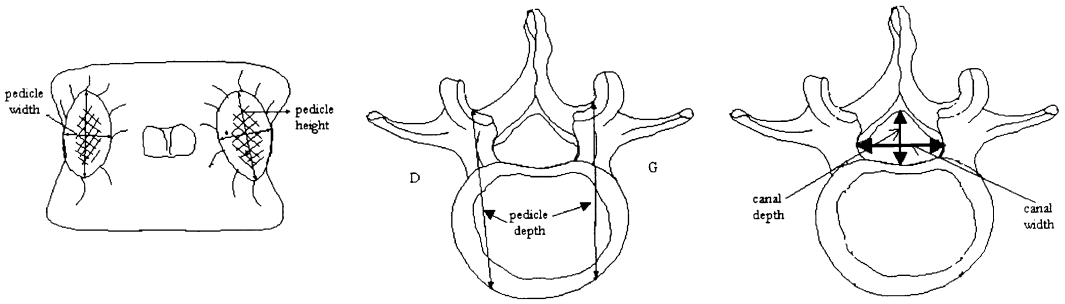

Fig. 9. Morphometric parameters used in our validation protocol.

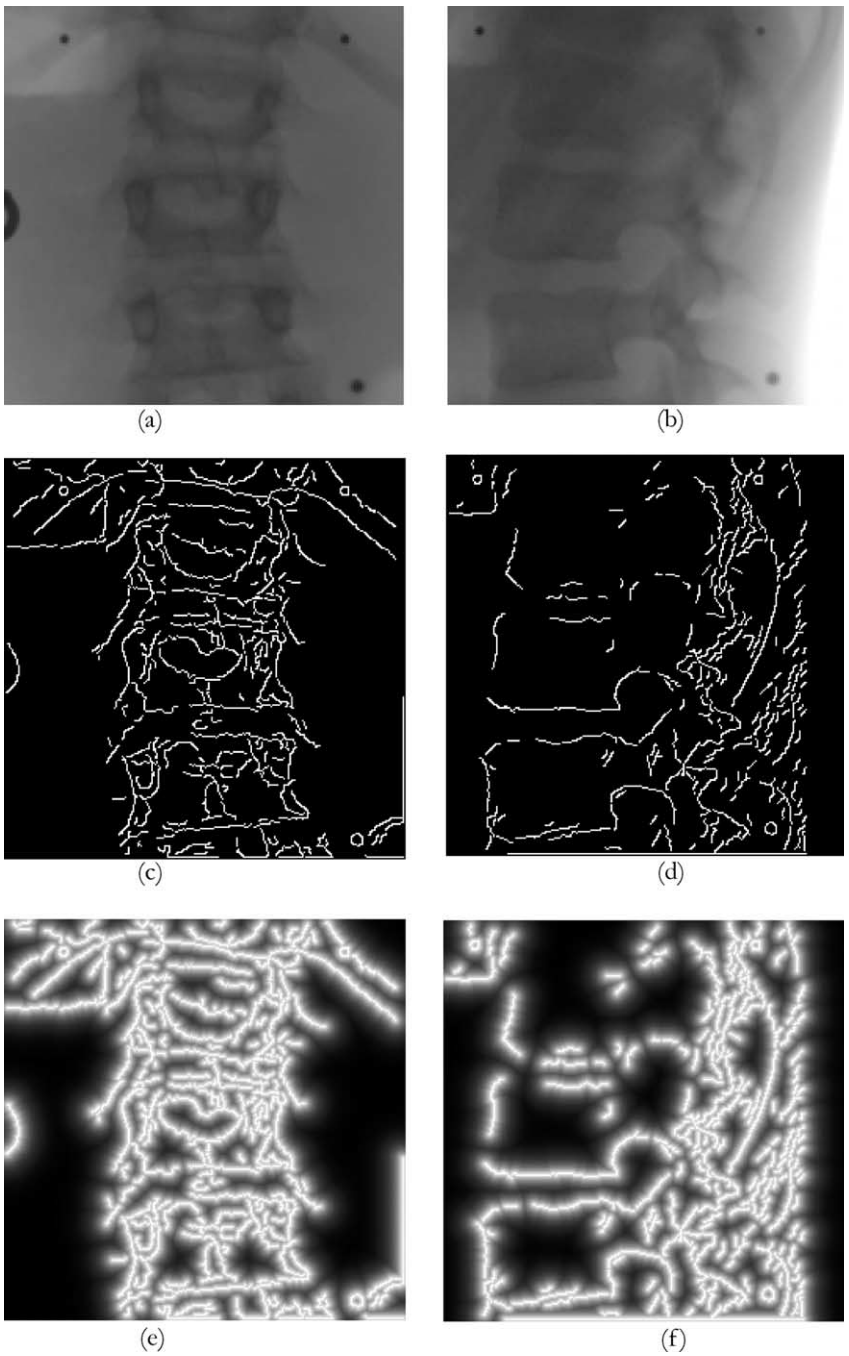

Fig. 10. Preprocessing: (a) postero-anterior image, (b) lateral image (256 × 256 pixels), (c) and (d) EDGE map using a Canny edge detector, (e) and (f) edge potential field.

Table 4
Normalized eigenvalues computed on a training set of 178 point models of 30 vertebrae obtained from the covariance matrix

L3 vertebra		T6 vertebra	
λ_i/V_T (%)	λ_i/V_T cumulated (%)	λ_i/V_T	λ_i/V_T cumulated (%)
26.46	26.46	27.62	27.62
19.44	45.90	24.06	51.68
8.95	54.85	12.37	64.04
7.95	62.80	9.55	73.59
6.89	69.69	6.49	80.09
6.22	75.91	5.42	85.50
4.88	80.80	4.19	89.69
3.88	84.68	2.80	92.49
3.45	88.12		
2.78	90.90		

image illustrates the superposition of various structures on a same plane and gives place to semi-transparent images.

5.3. Calibration

Calibration is a necessary step to compute the geometrical parameters of the radiological environment. The images are calibrated by a calibration object which is composed of two acrylic sheets parallel to the X-ray film plane. The two sheets contain embedded radiopaque spherical markers (55 steel balls) which are easily detectable on the radiographic images. The scene is calibrated using the 3D coordinates $(X, Y, Z)^T$ of each steel ball previously measured and their corresponding 2D observations $(x, y)^T$ to solve the following equation,

$$(x\ y\ \mu)^T = D(\vartheta, \kappa) \times (X\ Y\ Z)^T,$$

where μ is the X-ray tube distance ϑ and κ being, respectively, the scale and rotation vector [42].

5.4. Comparison protocol

We have validated our 3D/2D registration method on 57 scoliotic vertebrae (six lumbar vertebrae and 51 thoracic vertebrae) from 13 patients (13 pairs of radiographic images (postero-anterior and lateral views) of scoliotic spines). This comparison was made using the distance (mean, root mean square (RMS), and maximum) between a point from the reconstructed vertebra and the surface of the corresponding vertebra obtained with CT-scan, which was considered as the ground truth and whose accuracy is ± 1 mm [43].

We also considered five morphometric parameters related mostly to the dimensions of the pedicles and the spinal canal (Fig. 9). These measures can be useful for the surgeon because the pedicles are significant places for the installation of screws and hooks to allow rectification of the spinal column.

5.5. Experimental results

The mean vertebra shape of each vertebral level is computed from a sample of 30 normal vertebrae. The deformation modes of each vertebral level is computed on a sample of 30 scoliotic vertebrae.

We used the Canny edge detector to estimate the edge map which is then employed to estimate the *edge potential field* on the two radiographic views (Fig. 10). In our application, sigma = 1, mask size is 5×5, and the lower and upper thresholds are given by the unsupervised estimation technique proposed in [26].

In our application, we have chosen to take the number of deformation modes that allows representation of at least 90% of the admissible deformations for each type of vertebra. Table 4 shows that, for the L3 vertebra, the first 10 deformation modes integrate 90.90% of the deformations considered to be statistically admissible. For the T6 vertebra, the first eight deformation modes represent 92.49% of the deformations.

Besides, experiments have shown that the crude and rigid reconstruction procedure is not always a good initialization for the gradient-based optimization technique. As already stated in Section 3.5 and, in order to overcome this problem, our solution consists of placing the template at evenly-spaced positions and in deforming it according to a discretized set of translation orientations or scales (corresponding to rigid parameters) within a range of values around the initial estimate obtained by the rigid reconstruction procedure. These deformed template configurations can then be used to initialize a deterministic gradient descent algorithm. However, spacing between the template positions and the sampling of the transformations must be chosen judiciously: not too spaced out to cover all the significant local minima of the energy surface, and not too little spacing to avoid high computational requirements.

For the experiments, we have chosen $\beta = 1$ for the weighting factor penalizing the prior energy term with respect to external energy. The proposed method allows good registration of the vertebra. An example of projections of the shape of a L3 vertebra on postero-anterior and lateral radiographic images for a scoliotic patient is shown in Fig. 11.

The mean and the maximum error distance between the reconstructed model resulting from our 3D/2D registration method and the model resulting from CT-scan are, respectively, (0.71 ± 0.06), and (3.67 ± 0.80) mm for the lumbar vertebrae and (1.48 ± 0.27), and (6.44 ± 1.76) mm for the thoracic vertebrae. The results of comparison for 11 vertebral levels are given in Table 5. Pedicle width, pedicle height, pedicle depth, canal depth and canal width difference between

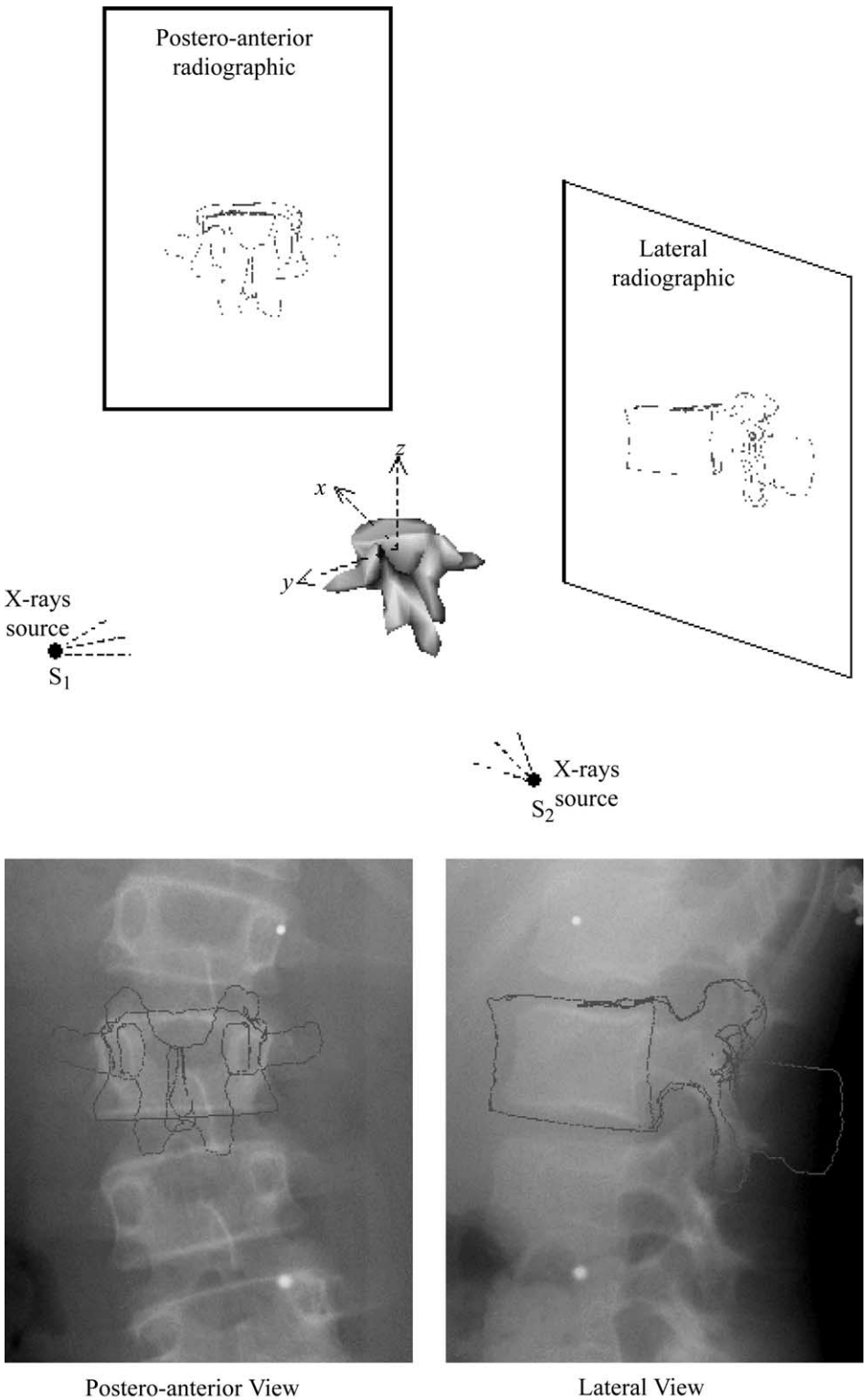

Fig. 11. Initial estimate of the mean shape of the vertebra on the two radiographic views by the proposed crude and rigid initial reconstruction method.

the reconstructed model resulting from our 3D/2D registration method and the model resulting from CT-scan are of the same order. The results of comparison for 11 vertebral levels are given in Table 6. Visual comparison between the reconstructed model resulting from our 3D/2D registration method and the model resulting from CT-scan for the L3 and T6 vertebrae is presented respectively in Figs. 12 and 13.

Table 5
Results on comparisons of 57 scoliotic vertebrae

Level	*N*	Mean error (mm)	Root mean square (mm)	Maximum error (mm)
T6	3	1.16 ± 0.07	0.20 ± 0.06	5.30 ± 1.04
T7	6	1.70 ± 0.29	0.22 ± 0.06	6.01 ± 0.57
T8	9	1.79 ± 0.18	0.25 ± 0.10	7.28 ± 4.00
T9	10	1.46 ± 0.32	0.24 ± 0.07	6.89 ± 1.61
T10	9	1.24 ± 0.31	0.23 ± 0.07	6.59 ± 0.61
T11	9	1.62 ± 0.52	0.21 ± 0.07	6.63 ± 1.28
T12	5	1.37 ± 0.21	0.16 ± 0.03	6.38 ± 1.17
L1	2	0.49 ± 0.03	0.04 ± 0.01	3.84 ± 0.21
L2	1	0.76 ± 0.12	0.05 ± 0.01	3.85 ± 0.90
L3	2	0.80 ± 0.02	0.06 ± 0.01	4.91 ± 0.15
L5	1	0.77 ± 0.06	0.04 ± 0.01	2.07 ± 1.26

6. Discussion and conclusion

We have presented an original statistical method of 3D/2D registration of scoliotic vertebrae using both the contours extracted from biplanar radiographic images and a priori knowledge of the geometric structure of each vertebra. This technique can also be viewed as an original 3D/2D reconstruction or segmentation model. The 3D/2D registration problem is stated as the minimization of a cost function for each vertebra and is solved with a gradient descent technique combined with a sampling strategy.

The results of validation presented above show that the reconstruction of lumbar vertebrae obtained by our 3D/2D registration method is more accurate than the 3D biplanar reconstruction method using non-stereo-corresponding points (NSCP) [7] and the 3D biplanar reconstruction method using corresponding points (DLT) [6,8]. The mean error is 0.7 mm for our method, 1.4 mm for NSCP, and 2.4 mm for DLT in [8], and 2.6 mm for DLT in [43]. Some maximum errors obtained on spinous processes are still high (i.e. maximum error is 3.9 mm for lumbar vertebra and 7.9 mm for thoracic vertebra) (Figs. 14 and 15). Even though these maxima correspond to points with no significant role in surgery planning, the accuracy of reconstruction is relatively acceptable with the results obtained by CT-scan which is considered as the more accurate reconstruction technique.

We note that the results are better for the lumbar vertebrae. For the thoracic vertebrae, the segmented contours are difficult to detect due to the presence of the ribs. Let us add that the size of the vertebra database, on which we performed a principal component analysis (PCA) to extract the deformations (considered to be statistically admissible), remains insufficient and does not certainly contain all the scoliotic deformations. Consequently, a large part of our reconstruction error results from the fact that some scoliotic deformations have not been modeled by PCA. Another part of our reconstruction error is due to the reconstruction error of the CT-scan technique considered as null in our validation protocol. Nevertheless, we can observe that the results obtained for morphometric parameters are nearly comparable with those obtained by CT-scan. Let us mention that these parameters are important for the surgical correction of scoliosis.

Let us recall that the surgical correction of scoliosis consists of correcting the scoliotic deformation by rotations and translations practiced at the level of the vertebrae and/or the level of the spine until a more normal alignment of the vertebrae is obtained. Correction consists of fixing the spine in this configuration using a metal rod supported by hooks and screws installed in the pedicles. Knowledge of the accurate sizes and geometry of these pedicles is thus crucial.

Let us note that the estimated global deformation parameters after reconstruction (i.e. parameter vector b, setting the amplitude of each deformation mode of the scoliotic deformations) and the measures of morphometric parameters can also be used to quantify the scoliosis, its nature or to analyze the improvement of orthopedic or surgical corrections.

To conclude, this method has demonstrated its efficiency and robustness. We strongly believe that a method which

Table 6
Results on point-to-surface comparisons of 57 scoliotic vertebrae

Level	*N*	Pedicle width (mm)	Pedicle height (mm)	Pedicle depth (mm)	Canal depth (mm)	Canal width (mm)
T6	3	0.43 ± 0.28	0.68 ± 0.22	0.71 ± 0.14	0.36 ± 0.45	0.53 ± 0.47
T7	6	1.03 ± 0.46	1.03 ± 0.55	1.33 ± 0.52	0.97 ± 0.64	1.42 ± 0.44
T8	9	1.34 ± 0.94	1.14 ± 0.63	1.44 ± 0.37	0.91 ± 0.50	0.59 ± 0.44
T9	10	1.15 ± 0.63	0.99 ± 0.81	1.59 ± 0.40	0.95 ± 0.72	1.00 ± 0.63
T10	9	1.04 ± 0.61	1.05 ± 0.66	1.28 ± 0.48	1.32 ± 0.59	1.36 ± 0.88
T11	9	1.06 ± 0.68	1.22 ± 0.71	1.30 ± 0.63	1.40 ± 0.52	0.96 ± 0.65
T12	5	1.12 ± 0.46	0.88 ± 0.63	1.12 ± 0.59	1.23 ± 0.71	1.06 ± 0.36
L1	2	0.26 ± 0.06	0.18 ± 0.08	0.22 ± 0.19	0.11 ± 0.05	0.02 ± 0.01
L2	1	0.27 ± 0.05	0.50 ± 0.09	0.17 ± 0.09	0.41 ± 0.11	0.14 ± 0.10
L3	2	0.22 ± 0.25	0.30 ± 0.17	0.31 ± 0.18	0.38 ± 0.34	0.21 ± 0.25
L5	1	0.25 ± 0.15	0.03 ± 0.01	0.29 ± 0.15	0.04 ± 0.02	0.61 ± 0.31

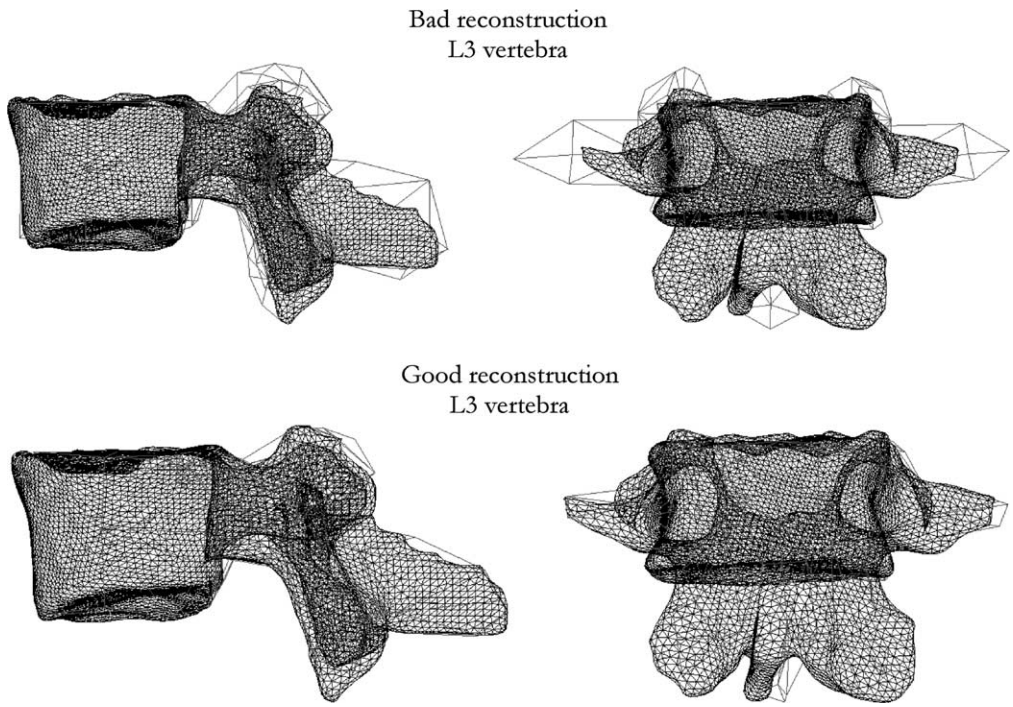

Fig. 12. Visual comparison between 3D reconstruction using our 3D/2D registration method (red lines) and reference CT-scan (black lines) for the L3 vertebra.

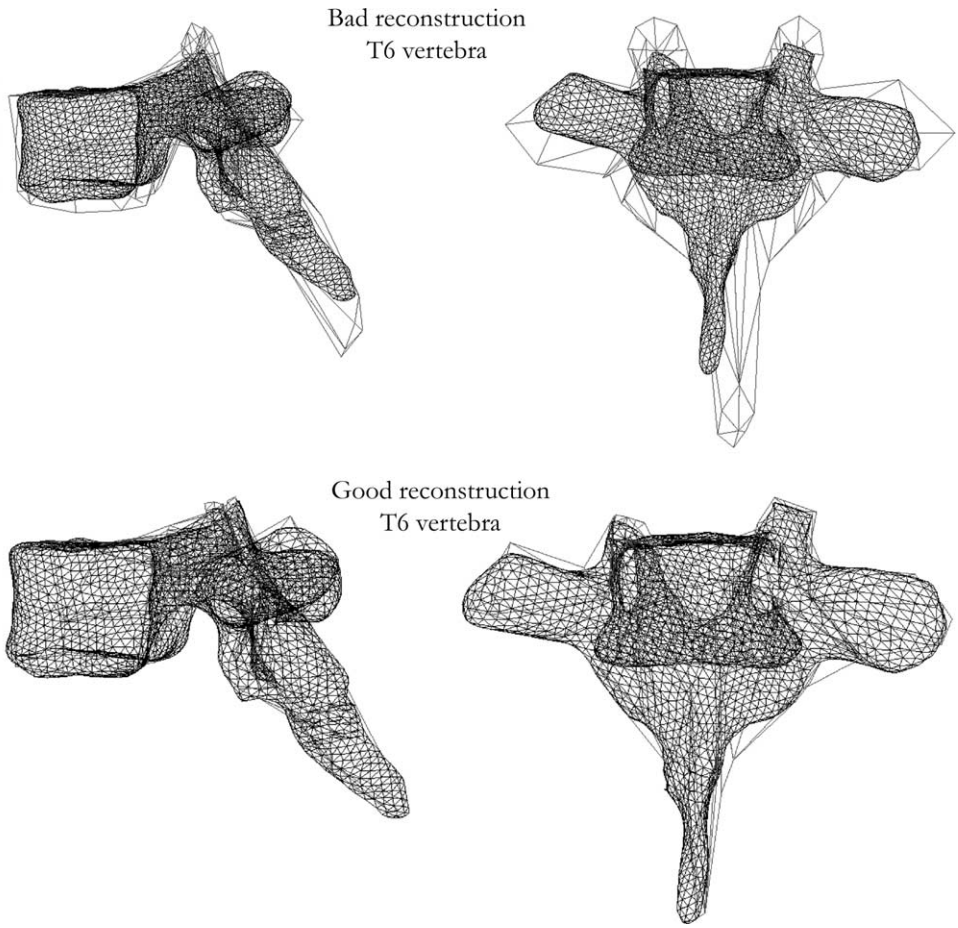

Fig. 13. Visual comparison between 3D reconstruction using our 3D/2D registration method (red lines) and reference CT-scan (black lines) for the T6 vertebra.

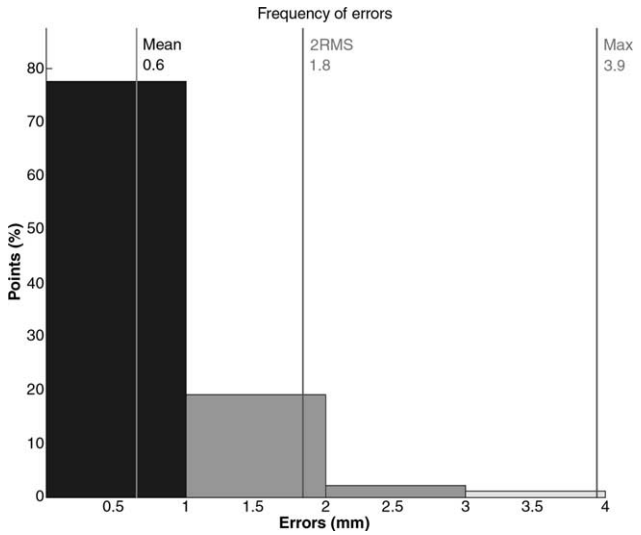

Fig. 14. Maximum and mean errors for reconstructed L3 vertebra.

gives results almost equal to those obtained by using more than 500 CT images for a whole spine but based on only two standard X-ray images is quite original, important, and interesting.

It is interesting for the quantity of data to be acquired, processed and managed. For example, two plain digital Fuji X-rays require 15 Mbytes (1,760 × 2,140 × 2 bytes) of storage in comparison to 260 Mbytes (512 × 512 × 2 bytes × 500 slices).

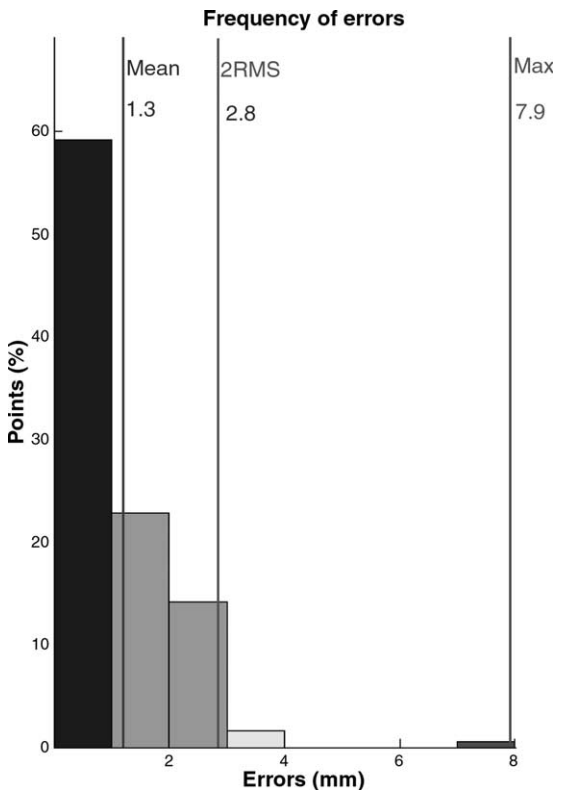

Fig. 15. Maximum and mean errors for reconstructed T6 vertebra.

It is important for the quantity of radiation received by the patient. With the generalization of multi-detector spiral CT, patients will be more and more exposed to radiation and a method that can keep this amount of radiation as low as possible is also quite important and has to be considered. It becomes especially important when we deal with young scoliotic patients who will be exposed to multiple diagnostic radiographic examinations during their childhood and adolescence. In Ref. [44], a retrospective study confirmed that multiple radiographic examinations may increase the risk of breast cancer among women with scoliosis. Another important point is that scoliosis must be evaluated when the patient is in a standing position, which is impossible with standard CT scanners.

The proposed method remains sufficiently general to be applied to other medical reconstruction problems (i.e. rib cage, pelvis, knee, etc.) for which the database of this anatomical structure is available (with two or several radiographic views). We now intend to improve the proposed method by integrating a region homogeneity term in the energy function related to this statistical reconstruction approach, to refine the statistical model by local deformations, and to use a more efficient global optimization technique.

7. Summary

We propose a new 3D/2D registration method for vertebrae of the scoliotic spine, using two conventional radiographic views (postero-anterior and lateral), and a priori global knowledge of the geometric structure of each vertebra. This geometric knowledge is efficiently captured by a statistical deformable template integrating a set of admissible deformations, expressed by the first modes of variation in KL expansion, of the pathological deformations observed on a representative scoliotic vertebra population. The proposed registration method consists of fitting the projections of this deformable template with the preliminary segmented contours of the corresponding vertebra on the two radiographic views. The 3D/2D registration problem is stated as the minimization of a cost function for each vertebra and solved with a gradient descent technique. Registration of the spine is then done vertebra by vertebra. The proposed method efficiently provides accurate 3D reconstruction of each scoliotic vertebra and, consequently, it also provides accurate knowledge of the 3D structure of the whole scoliotic spine. This registration method has been successfully tested on several biplanar radiographic images and validated on 57 scoliotic vertebrae. This method has demonstrated its efficiency and robustness. We strongly believe that a method which gives results almost equal to those obtained by using more than 500 CT images for a whole spine but based on only two standard X-ray images is quite original, important, and interesting. It is interesting for the quantity of data to be acquired, processed and managed. For example, two

plain digital Fuji X-rays require 15 Mbytes ($1760 \times 2140 \times 2$ bytes) of storage in comparison to 260 Mbytes ($512 \times 512 \times 2$ bytes $\times$ 500 slices). It is important for the quantity of radiation received by the patient. With the generalization of multi-detector spiral CT, patients will be more and more exposed to radiation and a method that can keep this amount of radiation as low as possible is also quite important and has to be considered. It becomes especially important when we deal with young scoliotic patients who will be exposed to multiple diagnostic radiographic examinations during their childhood and adolescence. Another important point is that scoliosis must be evaluated when the patient is in a standing position, which is impossible with standard CT scanners. The proposed method remains sufficiently general to be applied to other medical reconstruction problems (i.e. rib cage, pelvis, knee, etc.) for which the database of this anatomical structure is available (with two or several radiographic views). We now intend to improve the proposed method by integrating a region homogeneity term in the energy function related to this statistical reconstruction approach, to refine the statistical model by local deformations, and to use a more efficient global optimization technique.

Acknowledgements

The authors thank the Natural Sciences and Engineering Research Council of Canada, Canadian Foundation for Innovation, Valorisation Recherche Québec and the Biospace Company, Paris, France, for supporting this study.

References

[1] Brown LG. A survey of image registration techniques. ACM Comput Survey 1992;24(4):325–76.
[2] Van den Elsen PA, Maintz JBA, Pol E-JD, Viergever MA. Medical image matching—a review with classification. IEEE Engng Med Biol 1993;12(4):26–39.
[3] Lavallée S. Registration for computer integrated surgery: methodology, state of the art. In: Taylor R, Lavallée S, Burdea G, Moesges R, editors. Computer integrated surgery. Cambridge, MA: MIT Press; 1995. p. 77–97.
[4] Maintz JBA, Viergever MA. A survey of medical image registration. Med Image Anal 1998;2(1):1–36.
[5] West J. Comparison and evaluation of retrospective inter-modality registration techniques. Comput Assist Tomogr 1997; http://cswww.vuse.vanderbilt.edu/image/registration.
[6] De Guise JA, Mallouche H, Dansereau J, Labelle H. Imaging techniques applied to spinal biomechanics. J Biomech 1995;7(3):135–44.
[7] Mitton D, Landry C, Veron S, Skalli W, Lavaste F, De Guise JA. 3D reconstruction method from biplanar radiography using non-stereocorresponding points and elastic deformable meshes. Med Biol Engng Comput 2000;38:133–9.
[8] Mitulescu A, Semaan I, De Guise JA, Leborgne P, Adamsbaum C, Skalli W. Validation of the non-stereocorresponding points stereoradiographic 3D reconstruction technique. Med Biol Engng Comput 2001;39:152–8.
[9] Cootes TF, Taylor CJ. Active shape model search using local grey-level models: a quantitative evaluation. In: Illingworth J, editor. Proceddings of the British Machine Vision Conference. BMVA Press; 1993. p. 639–48.
[10] Cootes TF, Page CJ, Jackson CB, Taylor CJ. Statistical grey level models for object localization and identication. Proceedings of the British Machine Vision Conference 1995;533–42.
[11] Marchant JA, Onyango CM. Fitting grey level point distribution models to animals in scenes. Image Vision Comput 1995;13(1):3–12.
[12] Cootes TF, Taylor CJ, Cooper DH, Graham J. Training models of shape from sets of examples. Proceedings of the British Machine Vision Conference, Berlin: Springer; 1992. p. 9–18.
[13] Kervrann C, Heitz F. Statistical deformable model-based segmentation of image motion. IEEE Trans Image Process 1999;8(4):583–8.
[14] Lorenz C, Krahnstöver N. Generation of point-based 3D statistical shape models for anatomical objects. Comput Vision Image Understand 2000;77:175–91.
[15] Fleute M, Lavallée S. Nonrigid 3D/2D registration of images using a statistical model. Medical image computing and computer-assisted intervention, Berlin: Springer; 1999. p. 138–47.
[16] Fleute M, Lavallée S. Building a complete surface model from sparse data using statistical shape models: application to computer assisted knee surgery system. Medical image computing and computer-assisted intervention, Berlin: Springer; 1998. p. 879–87.
[17] Cootes TF, Taylor CJ, Haslam J. The use of active shape models for locating structures in medical images. Image Vision Comput 1994; 12(6):355–65.
[18] Hill A, Thornman A, Taylor CJ. Model-based interpretation of 3D medical images. Proceedings of the British Machine Vision Conference, England: Guildford; 1993. 339-348.
[19] Hill A, Cootes TF, Taylor CJ. A generic system for image interpretation using exible templates. Proceedings of the British Machine Vision Conference, Leeds, England; 1992. p. 1–10.
[20] Hill A, Cootes TF, Taylor CJ, Lindley K. Medical image interpretation: a generic approach using deformable templates. J Med Inform 1994;19(1):47–59.
[21] Dubuisson-Jolly M, Lakshmanan S, Jain AK. Vehicle segmentation and classification using deformable templates. IEEE Trans Pattern Anal Mach Intell 1996;18(3):293–308.
[22] Hadamard J. Lectures on the Cauchy problem in linear partial differential equations. New Haven: Yale University Press; 1923.
[23] Kauffman C, De Guise JA. Digital radiography segmentation of scoliotic vertebral body using a deformable model. Int Soc Optical Engng 1997;3034:243–51.
[24] Horn BKP, Shao N. Closed form solutions of absolute orientation using orthonormal matrices. J Optical Soc Am 1988;5(7):1127–35.
[25] Jain AK, Zhong Y, Lakshmanan S. Object matching using deformable templates. IEEE Trans Pattern Anal Mach Intell 1996;18(3):267–78.
[26] Canny JF. A computational approach edge detection. IEEE Trans Pattern Anal Mach Intell 1986;8(6):679–97.
[27] Chien CH. Reconstruction and recognition of 3D objects from occluding contours and silhouettes. Report Thesis, Department of Electrical Computer Engineering, University of Texas, Austin; 1987.
[28] Ponce J, Chelberg D. Finding the limbs and cups of generalized cylinders. Int J Comput Vision 1987;1:195–210.
[29] Maes F, Vandermeulen D, Suetens P. Comparative evaluation of multi-resolution optimization strategies for multi-modality image registration by maximization of mutual information. Med Image Anal 1999;3(4):373–86.
[30] Thévenaz P, Unser M. An efficient mutual information optimizer for multi-resolution image registration. IEEE International Conference on Image Processing, 1:833-837, Chicago; 1998.
[31] Woods RP, Grafton ST, Holmes CJ, Cherry SR, Mazziotta JC. Automated image registration: I. General methods and intra-subject, intra-modality validation. J Comput Assist Tomogr 1998; 22:141–54.
[32] Woods RP, Grafton ST, Watson J, Sicotte NL, Mazziotta JC. Automated image registration: II. Intersubject validation of linear and non-linear models. J Comput Assist Tomogr 1998;22(1):153–65.

[33] Mignotte M, Collet C, Pérez P, Bouthemy P. Hybrid genetic optimization and statistical model-based approach for the classification of shadow shapes in sonar imagery. IEEE Trans Pattern Anal Mach Intell 2000;22(2):129–41.
[34] De Guise JA, Martel Y. 3D biomedical modeling: merging image processing and computer aided design. Proceedings of the IEEE EMBS 10th International Conference, New Orleans; 1988. p. 426–7.
[35] Lorusso A, Eggert DW, Fisher RB. A comparison of four algorithms for estimating 3D rigid transformations. Mach Vision Appl 1997;9: 272–90.
[36] Horn BKP. Closed-form solution of absolute orientation using unit quaternions. J Optical Soc Am 1987;4(4):629–42.
[37] Arun KS, Huang TS, Blostein SD. Least-square fitting of two 3D point sets. IEEE Trans Pattern Anal Mach Intell 1987;9(5):698–700.
[38] Walker M, Shao L. Estimating 3D location parameters using dual number quaternions. CVGIP: Image Understand 1991;54(3):358–67.
[39] Parent S, Labelle H, Skalli W, Latimer B, De Guise JA. Morphometric analysis of anatomic scoliotic specimens. Spine 2002;27(21):2305–11.
[40] Borgne PL, Skalli W, Stokes IAF, Maurel N, Beaupère G, Lavaste F. Three-dimensional measurement of a scoliotic spine. In: D'amico M, Merolli A, Santambroglio GC, editors. Three-dimensional analysis of spinal deformities (IOS). ; 1995. p. 219–24.
[41] Semaan I, Skalli W, Veron S, Templier A, Lasseau JP, Lavaste F. Quantitative three-dimensional anatomy of lumbar spine. Eur J Orthop Surg 2001;.
[42] Marzan GT. Rational design for close-range photogrammetry. PhD Thesis, Department of Civil Engineering, University of Illinois at Urbana-Champaign, USA; 1976.
[43] Aubin CE, Dansereau J, Parent F, Labelle H, De Guise JA. Morphometric evaluations of personalized 3D reconstructions and geometric models of the human spine. Med Biol Engng Comput 1997; 35:611–8.
[44] Doody MM, Lonstein JE, Stovall M, Hacker DG, Luckyanov N, Land CE. Breast cancer mortality after diagnostic radiography: findings from the US Scoliosis Cohort Study. Spine 2000;25(16):2052–63.

Said Benameur was born in Tizi-Ouzou, Algeria. He received the Diploma Engineer degree in computer engineering from the Mouloud Mammeri University in Tizi-Ouzou, Algeria in 1990, and MSc in computer science from University of Quebec at Montreal, Canada in 1998. From 1993 to 1996, he was Computer engineer at the Head quarters civil, Algeria; He is currently a candidate for the PhD degree in engineering at Engineering School, University of Quebec, Canada. His research interests include statistical methods for medical imaging, computer vision and its applications to medical imaging.

Max Mignotte received his Master of Sciences (Electronics and Telecommunications) (1992) and his DEA (postgraduate degree) in digital signal, image and speech processing from the INPG University, France (Grenoble), in 1993 and his PhD degree in electronics and computer engineering from the University of Bretagne Occidentale (UBO) and the digital signal laboratory (GTS) of the French Naval academy, France, in 1998. He was an INRIA postdoctoral fellow at the University of Montreal (DIRO), Canada (Que.), from 1998 to 1999. He was also a NSERC post-doctoral fellow, a teaching assistant and a lecturer at the University of Montreal from September 1999 to July 2000. He is currently with DIRO at Computer Vision and Geometric Modeling Lab as an Assistant Professor at University of Montreal. His current research interests include statistical methods and Bayesian inference for image segmentation (with hierarchical Markovian, statistical templates, or active contour models), parameters estimation, tracking, classification, deconvolution and restoration issues in medical or sonar imagery.

Stefan Parent is currently finishing his residency in Orthopaedic Surgery at Montreal University. Concomitantly, he is finishing his PhD Thesis on the Morphometric Analysis of Anatomic Scoliotic Specimens. Once his residency is finished, Dr Parent will do a two-year spinal deformity fellowship in San Diego, CA and Paris, France and continue research on the role of the intervertebral disk in scoliosis. Once his fellowship is finished, Dr Parent plans on returning to Montreal to become a Clinician–Scientist pursuing research and clinical work on Scoliotic Deformities.

Hubert Labelle was born in Montreal, Canada in 1952. He received a MD and completed his residency in orthopaedics at University of Montreal, followed by a 2-year fellowship in paediatric orthopaedics at Sainte-Justine Hospital in Montreal, Rancho Los Amigos Hospital in California and the A.I. Du Pont Institute in Delaware. Since 1982, he has been appointed in the department of surgery at University of Montreal and at Ste-Justine Hospital where he is currently Professor of surgery and Titular of the Movement Sciences Research Chair of Sainte-Justine Hospital and University of Montreal. His clinical work is focused on the evaluation and treatment of scoliotic deformities in children and adolescents. He is head of the musculosqueletal research group at Sainte-Justine Hospital Research Center and director of the 3D Scoliosis Laboratory. His research interests are concentrated on the 3D evaluation and treatment of scoliotic deformities, with a particular emphasis on computer assisted surgery, 3D design and evaluation of braces for the treatment of idiopathic scoliosis, and 3D evaluation and simulation of surgery for scoliotic deformities.

Wafa Skalli, Born in 1957, is a mechanical engineer, graduated from ENSAM in 1980, and PhD in mechanical engineering in 1983. She joined LBM ENSAM in 1988, where she is presently Professor and assistant director, in charge of research team Biomechanics and orthopaedy. Her research is oriented towards understanding mechanical behaviour of musculoskeletal system with the aim (1) to assess normal behavior and mechanisms of degradation, (2) to improve implants and (3) to provide clinical tools for diagnosis and orthopedic or surgical treatment planning. She works mainly on geometric and mechanical modelling, with a strong link to in vitro experimentation and to in vivo quantitative clinical investigation. Wafa Skalli is particularly involved in spine biomechanics and scoliosis, in collaboration with more than 10 clinical teams, particularly that of Pr J. Dubousset (Paris), and others in France, US, Canada, Lebanon, Japan, Spain,… She is presently member of IRSSD board (International Research Society for Scoliotic Deformities), honour member of ARGOS (European Association of Research Groups for spine OSteosynthesis), and member of various other societies or scientific evaluation pannels.

Jacques A. de Guise received his BSc degree (1977) in Electrical Engineering and his PhD degree (1984) in Biomedical Engineering from École Polytechnique of Montreal (Canada). He was a Natural Sciences and Engineering Research Council (NSERC) postdoctoral scholar at the Computer Vision and Robotics Laboratory of McGill University (Canada) from 1984 to 1986. He was a NSERC researcher fellow at the Institut de génie biomédical of the University of Montreal from 1896 to 1990. He is currently Professor at the Automated Production Department of the École de technologie supérieure of Montréal and Director of the Laboratoire de recherche en imagerie et orthopédie of the University of Montreal Hospital Research Centre. His current research interests are medical image processing, 3D medical imaging, 3D modelling of the musculoskeletal system and computer assisted surgery.